Journal of Power Sources 549 (2022) 232137

Contents lists available at ScienceDirect

Journal of Power Sources

journal homepage: www.elsevier.com/locate/jpowsour

Comparative analysis of HESS (battery/supercapacitor) for power smoothing of PV/HKT, simulation and experimental analysis

Antonio Cano [a], Paul Arévalo [a,b], Dario Benavides [b,c], Francisco Jurado [a,*]

[a] Department of Electrical Engineering, University of Jaén, 23700, EPS Linares, Jaén, Spain
[b] Department of Electrical, Electronics and Telecommunications Engineering (DEET), University of Cuenca, Cuenca, 010107, Ecuador
[c] Department of Electrical Engineering, University of Málaga, 29010, Smart Campus, Málaga, Spain

HIGHLIGHTS

- Photovoltaic and hydrokinetic systems in electrical distribution systems.
- Problems of power fluctuations due to the intermittence of renewable sources.
- Stability and quality of the power grid.
- A hybrid storage system with supercapacitors and lithium-ion batteries.
- Enhanced Linear Exponential Smoothing Method.

GRAPHICAL ABSTRACT

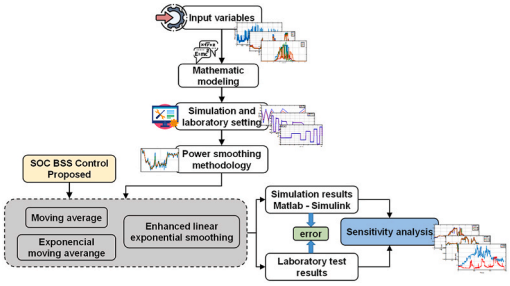

ARTICLE INFO

Keywords:
Photovoltaic
Hydrokinetic turbine
Battery
Supercapacitor
Power smoothing

ABSTRACT

Photovoltaic and hydrokinetic systems are increasing their penetration in electrical distribution systems. This leads to problems of power fluctuations due to the intermittence of renewable sources that could compromise the stability and quality of the power grid. To address this issue, this paper presents a feasibility study of three power smoothing methods for a photovoltaic-hydrokinetic system using laboratory equipment to optimally replicate the real behavior of this type of hybrid system. The proposed algorithms are based on a hybrid storage system with supercapacitors and lithium-ion batteries, several analyzes are presented based on technical and economic parameters.

The results demonstrate the feasibility of power smoothing methods for real systems, the comparison between the algorithms highlights the characteristics of the Enhanced Linear Exponential Smoothing Method, reducing the energy cost and regulating the point of common coupling voltage. Moreover, the sensitivity studies show that the energy exchange with the utility grid is affected according to the variations in the capacity of the batteries and the response to power smoothing can decrease or improve depending on the size of the supercapacitors.

* Corresponding author.
E-mail address: fjurado@ujaen.es (F. Jurado).

https://doi.org/10.1016/j.jpowsour.2022.232137
Received 29 May 2022; Received in revised form 28 August 2022; Accepted 17 September 2022
Available online 27 September 2022

Acronyms

SC	Supercapacitor
HKT	Hydrokinetic turbine
RES	Renewable energy sources
ESS	Energy storage system
BAT	Battery
HESS	Hybrid energy storage system
HRS	Hybrid renewable system
BSS	Battery storage system
DOD	Depth of discharge
WT	Wind turbine
PV	Photovoltaic
GA	Genetic algorithm
PSO	Particle swarm optimization
PCC	Point of common coupling
SOC	State of charge
Sets	Indexes and Functions
PS	Index of power smoothing method
Ξ	Set of the several power smoothing method
t	Index for time
ps	Index of the several power smoothing method
MAE	Mean absolute error
RMSE	Root mean squared error
MAPE	Mean absolute percentage error

Parameters and decisions variables

T	Number of time intervals
$P_{ps,t}^{PV}$	Electrical output power of PV for each power smoothing method and time t
λ^{PV}	Photovoltaic derating factor (%)
α_{pw}^{PV}	Temperature coefficient of power (%/°C)
T_{PS}^{PV}	Cell temperature in the photovoltaic array (°C)
T_{S}^{PV}	Cell temperature under standard test conditions (°C)
$I_{T,ps,t}^{PV}$	Photovoltaic current generated by the incident radiation in the cell at power smoothing method ps and time t (A)
$I_{S,ps,t}^{PV}$	Reverse saturation diode current at power smoothing method ps and time t (A)
$\gamma_{ps,t}^{PV}$	Rated capacity of the photovoltaic at power smoothing method ps and time t (kW)
$P_{ps,t}^{HKT}$	Electrical power output of hydrokinetic turbine
ρ^{ω}	Water density (kg/m^3)
A^{HKT}	Hydrokinetic turbine sweep surface (m^2)
$\alpha_{ps,t}$	River speed at configuration c and time t
ζ_{p}^{HKT}	Hydrokinetic turbine power coefficient
η^{HKT}	Hydrokinetic turbine efficiency
$E_{ps,t}^{SC}$	Output energy of supercapacitor at power smoothing method ps and time t (kWh)
C^{SC}	Capacitance of SC (F)
$V_{ps,t}^{SC}$	Voltage of SC at power smoothing method ps and time t (V)
$\eta_{ps,t}^{SC}$	Supercapacitor at power smoothing method ps and time t
$V_{ps,t}^{min}$	SC voltage lower limit at power smoothing method ps and time t (V)
$V_{ps,t}^{max}$	SC voltage upper limit at power smoothing method ps and time t (V)
$I_{ps,t}^{Ch,max}$	Maximum charge current allowed in SC at power smoothing method ps and time t (A)
$I_{ps,t}^{Dis,max}$	Maximum discharge current allowed in SC at power smoothing method ps and time t (A)
$P_{ps,t}^{SC}$	Power delivered by the SC at power smoothing method ps and time t (kW)
$P_{W,ps,t}^{SC}$	Power wasted internally by the SC at power smoothing method ps and time t (kW)
$P_{ps,t}^{BSS+}$	Output power of battery bank at power smoothing method ps and time t (kW) during charge process
$P_{ps,t}^{BSS-}$	Output power of battery bank at power smoothing method ps and time t (kW) during discharge process
$SOC_{ps,t}^{BSS}(k+1)$	State of charge of battery storage system at $k+1$ process in power smoothing method ps and time t
$SOC_{ps,t}^{BSS}(k)$	State of charge of battery storage system at k process in power smoothing method ps and time t
η_{inv}	Inverter efficiency
η_{BSS}^{ps}	Battery efficiency at power smoothing method ps
$P_{ps,t}^{BSS+}(k+1)$	Output power of battery bank at power smoothing method ps and time t (kW) during charge process in at $k+1$
$P_{ps,t}^{BSS-}(k+1)$	Output power of battery bank at power smoothing method ps and time t (kW) during discharge process in at $k+1$
ΔT	Time interval
$\underline{SOC}_{ps,t}^{BSS}$	Lower bound state of charge in BSS at power smoothing method ps and time t, in k process
$\overline{SOC_{ps,t}^{BSS}}$	Upper bound state of charge in BSS at power smoothing method ps and time t, in k process
$\overline{P_{BSS}^{ch}}$	Upper bound power operate during charge BSS
$\overline{P_{BSS}^{disch}}$	Upper bound power operate during discharge BSS
$SOC_{sdc,t}^{SC}$	State of charge in SC at power smoothing method ps and time t
$SOC_{sdc\ min,t}^{SC}$	Minimum state of charge in SC at power smoothing method ps and time t
$p_{c,t}^{HKT}$	Power delivered by the HKT at power smoothing method ps and time t
$E_{c,t}^{SC}$	Energy delivered by the SC at power smoothing method ps and time t
$P_{ps,t}^{g}$	Total power flow between grid an HRS at power smoothing method ps and time t
$P_{ps,t}^{g,b}$	Grid power to prosumers at power smoothing method ps and time t
$P_{ps,t}^{g,s}$	Prosumers to grid at power smoothing method ps and time t
$\overline{P_{ps,t}^{g,max}}$	The thermal capacity of the power link between the HRS and the grid at power smoothing method ps and time t
$P_{ps,t}^{smooth}$	Smoothed reference power grid at power smoothing method ps and time t
$P_{ps,t}^{HRES}$	Electric power generated by the hybrid system at power smoothing method ps and time t
$P_{ps,t}^{HESS}$	Power (absorbed) or discharged (injected) by the HESS at power smoothing method ps and time t
w	Averaging window
P_{t}^{Load}	Electrical power of demand
n	Time in seconds of testing
X_s	Simulated Value
X_l	Laboratory Value

1. Introduction

1.1. Motivation and incitement

Renewable energy in residential systems is increasingly promising, the price of energy from the utility grid can reach high costs depending on some variables, e.g. availability of resources, climate, etc., especially in peak demand. Photovoltaic (PV) and hydrokinetic (HKT) systems can help reduce the cost of electricity by being located close to customers, complementary an energy storage system decreases consumption from the grid during peak hours where energy costs are generally higher. This alternative could be feasible, however, the energy sent to the grid could not meet the quality standards of the electricity distribution companies, since PV and HKT present power fluctuations. The stability of the electrical system can be compromised if the number of users is large enough. It is because of that, an efficient method of power smoothing from renewable sources and the load is necessary, in this way, the indexes of energy quality and stability in the power system can be improved. It is important to point out that, with the purpose of determine the efficiency of method. In this paper, exhaustive analyzes must be done comparing the several methods, within the computational and experimental field.

1.2. Literature review

The battery storage system (BSS) has gained wide applicability in residential renewable systems connected to the grid especially in developing countries [1]. The most widely used technologies today are lead acid and lithium ion. These first ones have improved with VRLA technology with a life expectancy of 5–8 years, a depth of discharge (DOD) of up to 20% and a maximum expected cycles of 3000 cycles [2]. Lithium ion batteries, having a longer life expectancy (approximately 10 years) than lead acid and a higher energy density, have expanded in the market for residential photovoltaic applications [3]. The BSS in power smoothing applications play an important role, during cloudy days the PV systems produce power peaks that can harm the stability of the utility grid. Formerly, power smoothing methods included resistors that dissipated the surplus electricity of PV avoiding rising peaks, the disadvantage of these techniques lies in the inability to smooth out the descending power peaks [4]. Rayee Ahmad et al. proposes a framework for optimizing the integration of BSS to a grid-connected PV system, the BSS model provides an annual energy loss reduction of 25.69% [5]. Similarly, in Ref. [6], the authors present a predictive control of neural networks to smooth solar energy fluctuations with BSS based on genetic algorithm (GA) and particle swarm optimization (PSO). The results show that the power smoothing methods reduce the flicker at the point of common coupling (PCC). The articles cited above are based on computational simulations and lack experimental evidence to refute or verify their operation.

To troubleshoot power smoothing in PV systems, several authors have proposed various techniques using BSS and supercapacitors (SC). Indeed, Ref. [7], the author shows a control strategy of BSS and SC, creating a hybrid energy storage system (HESS) to diminish photovoltaic power oscillations considering the reduction of PV output, the results show that the technique presented extends the lifespan of lithium ion batteries by reducing their charge/discharge cycles. Likewise, Ma. Wei et al. [8] has considered the reduction of the HESS capacity through coordinated control that smoothest the power peaks by correcting the state of charge (SOC) of BSS, the results show the cost reduction of the PV plant and BSS. In similar way, these studies are based on a single method without considering laboratory tests or real data, which may not adhere to the real behavior of the systems. In this sense, Mukalu Sandro et al. [9], use real solar irradiance data in a South African community to model a power smoothing technique in a renewable hybrid PV/BSS system integrated in the utility grid with a predictive control method, in order to eliminate fast variations of energy absorbed by the BSS and injected into the grid. Simulations performed a large PV plant maintaining the electrical parameters within the norms of the electric power company and improved the quality of energy generated by intermittent renewable energy sources (IRES), and extension of BSS life. However, to ensure the viability of this technique, it is necessary to compare with respect to various power smoothing methods, considering several technical and economic aspects that demonstrate their viability. Additionally, there are several types of BSS that can be used in power smoothing techniques, the most used technologies are lead acid and lithium ion, this way, in Ref. [10] the authors present an energy leveling strategy for a connected PV plant to the grid using vanadium redox flow batteries, the effectiveness of the control lies in operating the battery at high levels. Similarly, Ref. [11] presents a novel method of reducing power fluctuations based on dynamic control strategies with BSS and SC.

Some of the most used methods in the literature to smooth power peaks are based on Moving Average (MA), to apply this technique it is recommended to use lithium ion batteries to achieve the ramp speed limit [12]. Likewise, the Exponential Moving Average (EMA) and Enhanced Linear Exponential Smoothing Method (ELES) are techniques that are not widely used by scientists currently; however, the results of related studies are promising. Nevertheless, few authors have studied this technique from a laboratory and compared it with other methods [13].

On the other hand, hydrokinetic turbines (HKT) have been promoted for residential use in areas with ideal river speeds, the random behavior of this resource means that the output power is not constant and must be corrected to a lesser extent than PV. From a review of the extensive literature available, few studies of HKT fluctuations have been found, mainly applied to ocean currents, where the behavior of a unidirectional river flow is different [14,15]. In this way, the investigation of the current literature on methods to power smoothing of a renewable hybrid system have yielded the following research questions:

- ¿What makes a power smoothing method of hybrid renewable PV/HKT grid-connected system based on BSS/SC feasible?
- ¿Are laboratory tests like simulations?
- ¿What type of power smoothing method is recommended?
- ¿What is the advantage of monitoring the state of charge of the BSS/SC during power smoothing?
- ¿What is the response of the BSS life expectancy when implementing a SC in power smoothing?
- ¿ Does the voltage at PCC with a power smoothing method improve?
- What happens to the daily energy cost of consumers with respect to the utility grid?

1.3. Contribution and paper organization

To answer the research questions raised in this paper, a comprehensive analysis of various power smoothing methods for PV/HKT/BSS/SC connected to grid is proposed.

Three algorithms studied in the literature are presented, such as MA, EMA and ELES. This comparison aims to prove or refute the results obtained with the classical methods. This paper goes further as it compares the simulated results in Matlab - Simulink with respect to laboratory systems. In addition, a control of the SOC of the BSS/SC is presented. In summary, the main contributions of this paper are:

- Comparative feasibility study of three power smoothing methods for PV/HKT/BSS/SC/Grid system.
- Laboratory tests of the methods considering the respective restrictions.
- Sensitivity analysis regarding the capacity of batteries and supercapacitors are presented.
- Application of the algorithms: MA, EMA and ELES for intermittent renewable sources.
- Voltage response at PCC is analyzed.
- SC charge/discharge cycles are studied.

2. Methodology

The methodology used in this study is illustrated in Fig. 1.

Input data is used to perform the mathematical modeling that serves as the basis for the simulation in Matlab - Simulink. Subsequently, power smoothing is done using three algorithms and compared with the laboratory results. Finally, several sensitivity analyzes are presented.

2.1. Input data and background

Solar irradiance and ambient temperature have been obtained by a meteorological station of the University of Cuenca. The river speed has been measured for a hydrological station. Then, the electricity demand corresponds from a group of common residential houses located in the south of Ecuador, in the city of Cuenca [16,17]. The input data can be seen in Fig. 2.

On the other hand, with the purpose of study the power smoothing methods in more detail, it is necessary to represent the input variables in intervals of seconds as shown in Fig. 3.

Therefore, Fig. 4 expresses the input data for three randomly selected days during a year.

The input data includes technical parameters of the sources and storage system, which are shown in Table 1 [16]. These are mathematically modeled below.

2.2. Mathematical modeling

2.2.1. Photovoltaic system

The PV power output is expressed in Eq. (1) [18].

$$P_{ps,t}^{PV} = \gamma_{ps,t}^{PV}.\lambda^{PV}.\left(\frac{I_{T,ps,t}^{PV}}{I_{S,ps,t}^{PV}}\right).\left[1+\alpha_{pw}^{PV}.\left(T_{PS}^{PV}-T_{S}^{PV}\right)\right];\ \forall t \in T,\ \forall ps \in PS \cup \Xi \quad (1)$$

2.2.1.1. Constraints. If $T_{PS}^{PV} < T_{S}^{PV}$, the PV system produces electrical energy due to the term α_{pw}^{PV} generally is < 0. To avoid indeterminacy, $I_{S,ps,t}^{PV} \neq 0$.

2.2.2. Hydrokinetic turbine

The electrical power output of HKT is expressed in Eq. (2) [19].

$$P_{ps,t}^{HKT} = \left(\frac{1}{2}.\rho^{\omega}.A^{HKT}.\alpha_{ps,t}^{3}.\zeta_{p}^{HKT}.\eta^{HKT}\right);\ \forall t \in T,\ \forall ps \in PS \cup \Xi \quad (2)$$

2.2.2.1. Constraints. The starting speed is 1 m/s and the cutting speed is 3 m/s, therefore: $1 \leq \alpha_{ps,t}^{3} \leq 3$.

2.2.3. Supercapacitor modeling

The output energy of SC is calculated with the Eq. (3) [20].

$$E_{ps,t}^{SC} = \frac{1}{2}.C^{SC}.\left(V_{ps,t}^{max} - V_{ps,t}^{min}\right)^{2};\ \forall t \in T,\ \forall ps \in PS \cup \Xi \quad (3)$$

The efficiency of the SC is expressed in Eq. (4).

$$\eta_{ps,t}^{SC} = \frac{P_{ps,t}^{SC}}{P_{ps,t}^{SC} + P_{W,ps,t}^{SC}};\ \forall t \in T,\ \forall ps \in PS \cup \Xi \quad (4)$$

The state of charge (SOC) is calculated through Eq. (5).

$$SOC_{ps,t}^{SC} = \frac{V_{ps,t}^{SC} - V_{ps,t}^{min}}{V_{ps,t}^{max} - V_{ps,t}^{min}};\ \forall t \in T,\ \forall ps \in PS \cup \Xi \quad (5)$$

2.2.3.1. Constraints. The values of maximum and minimum voltages of the SC depend on the inverter. The Eqs. (6) and (7) express the restrictions of the SC.

$$V_{ps,t}^{min} < V_{ps,t}^{SC} < V_{ps,t}^{max};\ \forall t \in T,\ \forall ps \in PS \cup \Xi \quad (6)$$

$$I_{ps,t}^{Ch,max} < I_{ps,t}^{SC} < I_{ps,t}^{Dis,max};\ \forall t \in T,\ \forall ps \in PS \cup \Xi \quad (7)$$

The test carried out shows the supercapacitors with a power of 15 kW, at a capacity of 13 F, the inverter voltage is between 640 V and 440 V.

2.2.4. Battery modeling

The power of the battery bank can be expressed as $P_{ps,t}^{BSS+}$ (charge) and $P_{ps,t}^{BSS-}$ (discharge). The variation of SOC of BSS during charge and discharging is expressed by Eq. (8) [9].

$$SOC_{c,t}^{BSS}(k+1) = SOC_{ps,t}^{BSS}(k) + \eta_{inv}.\eta_{BSS}^{ps}.P_{ps,t}^{BSS+}(k+1).\Delta T - \frac{1}{\eta_{inv}.\eta_{BSS}^{d}}P_{ps,t}^{BSS-}(k+1) \quad (8)$$

2.2.4.1. Constraints. The state of charge (SOC) of the battery for any time is limited by Eq. (9-11):

$$\underline{SOC_{ps,t}^{BSS}} < SOC_{ps,t}^{BSS}(k) < \overline{SOC_{ps,t}^{BSS}}, \forall t \in T,\ \forall ps \in PS \cup \Xi \quad (9)$$

$$0 \leq P_{ps,t}^{BSS+}(k) < \overline{P_{BSS}^{ch}} \Big/ \eta_{inv},\ \forall t \in T,\ \forall ps \in PS \cup \Xi \quad (10)$$

$$0 \leq P_{ps,t}^{BSS-}(k) < \eta_{inv} \Big/ \overline{P_{BSS}^{disch}},\ \forall t \in T,\ \forall ps \in PS \cup \Xi \quad (11)$$

The following constraint (Eq. 12 and (13) prevents simultaneous charging and discharging of batteries:

$$P_{ps,t}^{BSS+}(k).P_{ps,t}^{BSS-} = 0 \forall t \in T,\ \forall ps \in PS \cup \Xi \quad (12)$$

Therefore;

$$P_{ps,t}^{BSS} = P_{ps,t}^{BSS-} - (k).P_{ps,t}^{BSS+} = 0;\ \forall t \in T,\ \forall ps \in PS \cup \Xi \quad (13)$$

The lithium ion batteries used for this experiment have a power of 88 kW with a capacity of 436.56 kWh (680 Ah y 642 V).

2.2.5. Utility grid modeling

If renewable sources deliver electricity to the utility grid, it is expressed by $P_{ps,t}^{g,s}$, On the contrary, if the electricity flows from the utility grid to the load it is expressed by $P_{ps,t}^{g,b}$. The maximum limit of energy transmission is expressed by $\overline{P_{ps,t}^{g,max}}$, this boundary conditions are expressed in Eq. 14 and 15 [20]:

$$P_{ps,t}^{g,s} \leq \overline{P_{ps,t}^{g,max}},\ \forall t \in T,\ \forall ps \in PS \cup \Xi \quad (14)$$

$$P_{ps,t}^{g,b} \leq \overline{P_{ps,t}^{g,max}},\ \forall t \in T,\ \forall ps \in PS \cup \Xi \quad (15)$$

Constraint bidirectional flow es shown by Eq. (16);

$$P_{ps,t}^{g,s}.P_{ps,t}^{g,b} = 0,\ \forall t \in T,\ \forall ps \in PS \cup \Xi \quad (16)$$

The net flow of energy is expressed by Eq. (17)

$$P_{ps,t}^{g} = P_{ps,t}^{g,b} - P_{ps,t}^{g,b} = 0,\ \forall t \in T,\ \forall ps \in PS \cup \Xi \quad (17)$$

2.3. Setting laboratory tests and simulation

Based on the equipment installed in the microgrid laboratory of the University of Cuenca (Table 1). The simulations have been developed in Matlab - Simulink with the following results shown in Fig. 5 [16].

As can be seen, the computational model adjusts precisely to the real behavior of the components.

2.4. Power smoothing methodology

The power sent to the utility grid must be adjusted to the reference value of the controller, the power smoothing algorithm is able to mea-

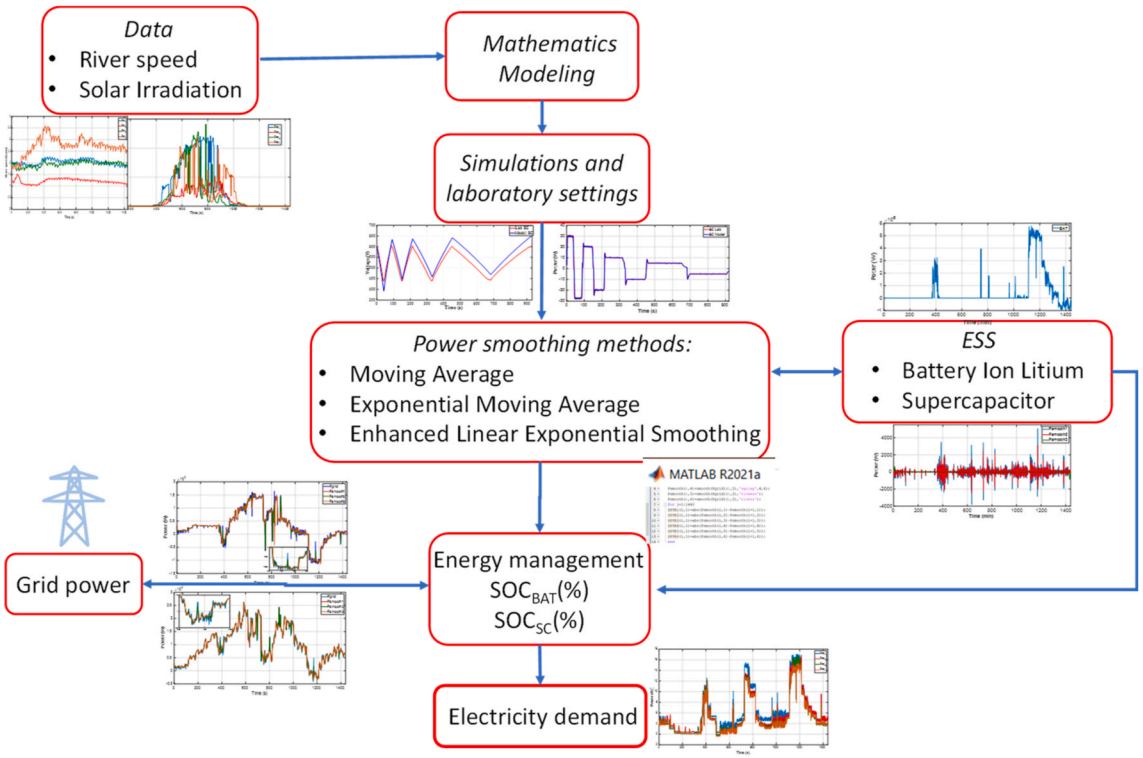

Fig. 1. Schematic representation of the proposed computational and experimental analysis.

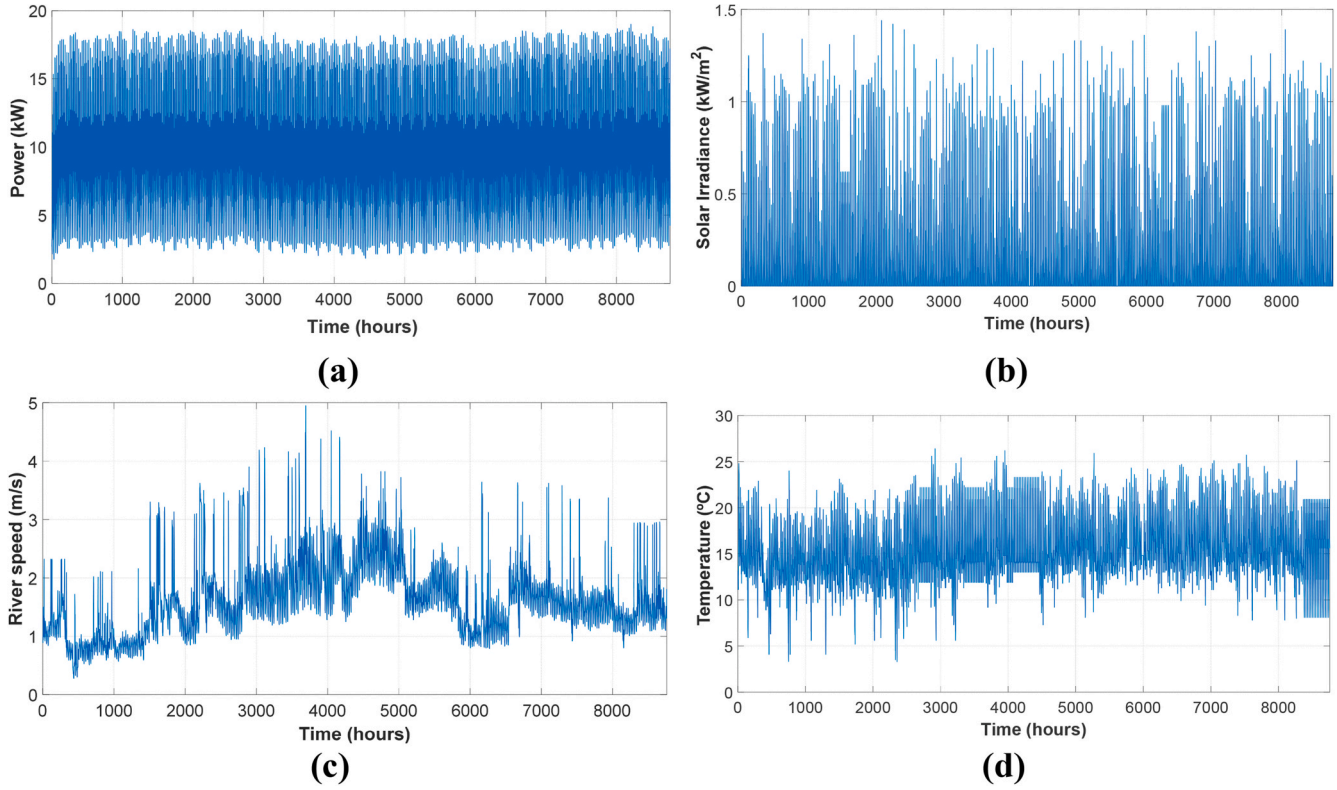

Fig. 2. Annual input data; (a) electricity demand, (b) solar irradiance (c) river speed and (d) ambient temperature.

sure the power generated and coordinate the HESS storage system with the HRES renewable sources to obtain the new smoothed power. Thus, the power sent to the utility grid is expressed with Eq. (18):

$$P_{ps,t}^{smooth} = P_{ps,t}^{HRES} \mp P_{ps,t}^{HESS},\ \forall t\ \in T,\ \forall ps\ \in PS \cup \Xi \tag{18}$$

Therefore, based on the analyzed renewable sources (PV/HKT), several power smoothing methods are analyzed. Generally, the literature discusses algorithms with filters or moving averages (MA). Moreover, details of other less well-known and efficient smoothing methods

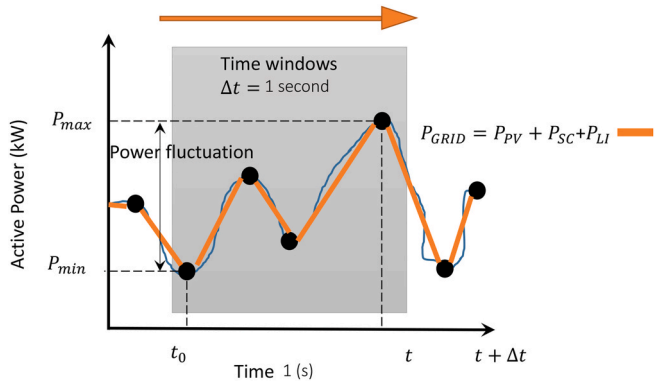

Fig. 3. Time window and chronology of the temporal analysis of power smoothing.

are presented, i.e., exponential moving average (EMA), enhanced linear exponential smoothing (ELES). In this regard. Fig. 6 shows the control diagram of the proposed comparison of power smoothing methods [21, 22].

2.4.1. Moving average method

The MA algorithm uses average values in a given time series. For the control, $P_{ps,t}^{HESS}$ at a certain instant *k*th depends on the previous values of $P_{ps,t}^{HRES}$ within the averaging window (w). It can be expressed by Eq. (19) [23]:

$$P_{ps,t}^{HESS}(k) = \frac{\sum_{i=0}^{w-1} P_{HRES}(k-i)}{w} - P_{HRES}(k) \tag{19}$$

Table 1
Main parameters of the proposed HRES.

Component	HKT	SC	Converter	PV	BSS
Origin	Smart hydro	Maxwell	MG5KTL	Artesa	Samsung
Specification Size	5 kW each unit	56 V 130 F variable	50 kW each unit	250 Wp each unit	436 kWh Battery bank

2.4.2. Exponencial moving average method

If an exponential weighting is performed on the MA algorithm, a higher prioritization of recent samples is obtained, this method is called exponential moving average (EMA), and is calculated with Eq. (20) [24]:

$$P_{ps,t}^{HESS}(k) = \sum_{n=0}^{w-1} \alpha[(1-\alpha)^n P_{HRES}(k-n)] - P_{HRES}(k) \tag{20}$$

where n = {0, 1, 2, …, w - 1} and the factor α is the smoothing coefficient, which is between 0 and 1. The weight terms (1- α) are reduced exponentially so that the current data is more significant than previous data.

2.4.3. Enhanced Linear Exponential Smoothing Method

In order to obtain greater precision with respect to MA and EMA, Enhanced Linear Exponential Smoothing Method are performed, this increases the mathematical complexity of the algorithm, Eq. (21) mathematically expresses the ELES method [25]:

$$P'_{HRES}(k) = \varrho P'_{HRES}(k) + (1-\varrho) P'_{HRES}(k-1)$$

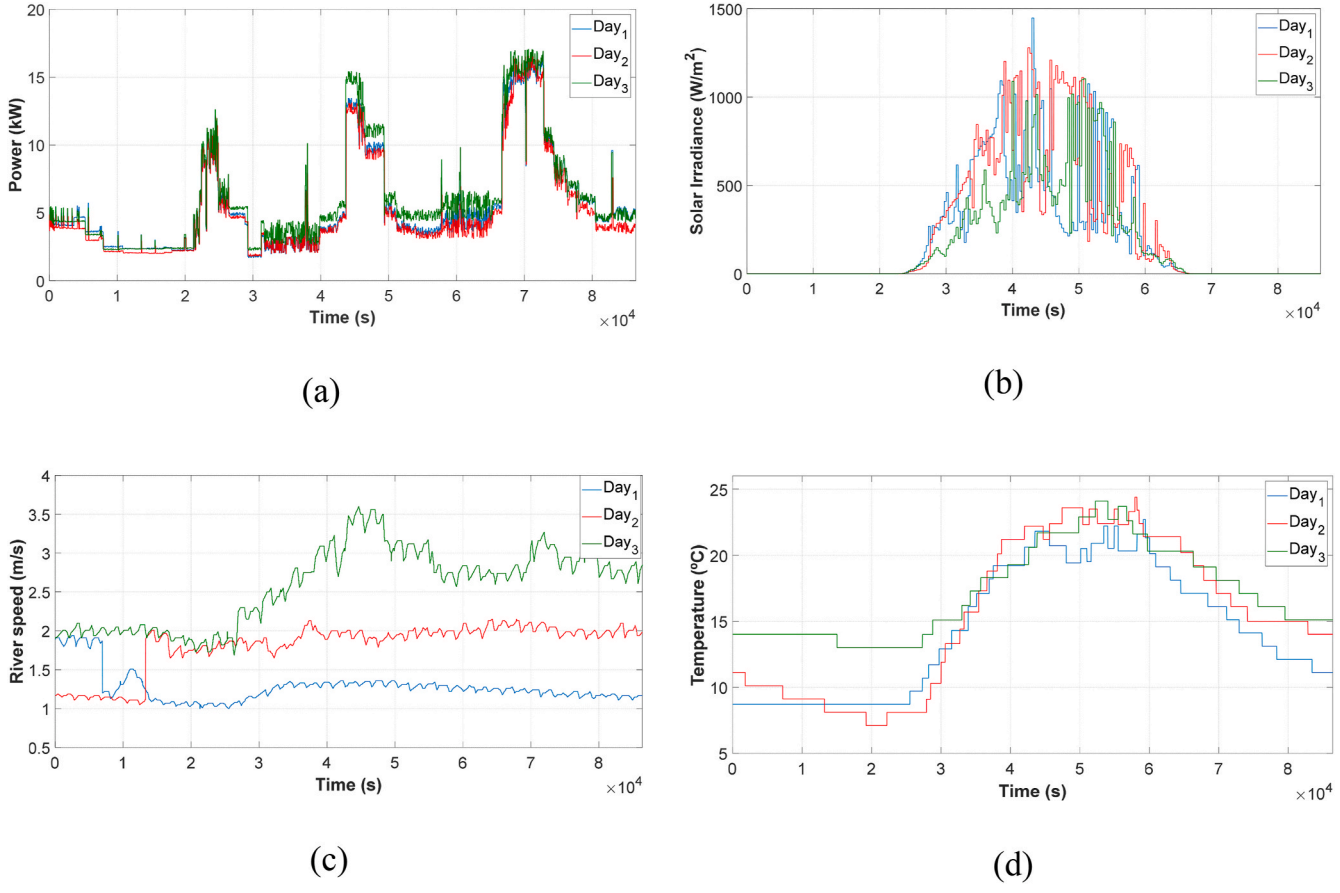

Fig. 4. Daily input data; (a) electricity demand, (b) solar irradiance (c) river speed (d) ambient temperature.

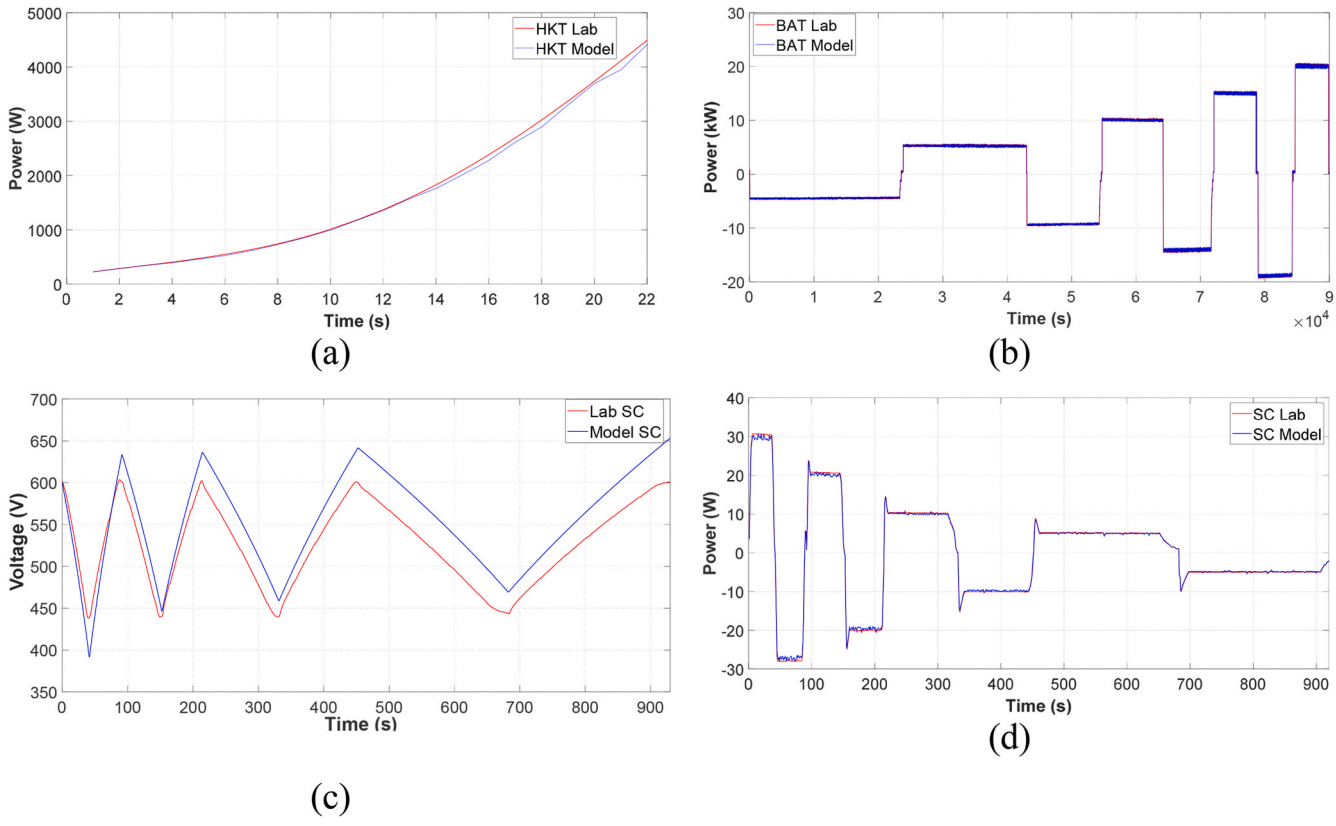

Fig. 5. Setting between computational models and real models: (a) HKT, (b) BSS, (c) SC voltage and (d) SC power output.

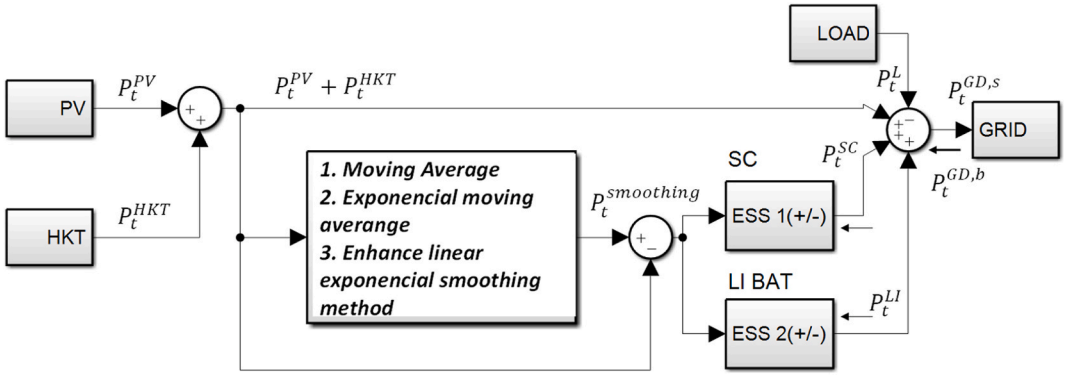

Fig. 6. Control diagram of power smoothing methods.

$$P''_{HRES}(k) = \varrho P'_{HRES}(k) + (1-\varrho)P''_{HRES}(k-1)$$

$$P_{ESS}(k) = 2P'_{HRES}(k) - P''_{HRES}(k-1) - P_{HRES}(k) \tag{21}$$

where P'_{HRES} and P''_{HRES} are auxiliary variables to calculate the double complementary filter. The smoothing factor (ϱ) has a value between 0 and 1.

2.5. Energy management

This section presents the mathematical representations of power flows considering the technical and boundary conditions.

The energy produced by HRES supplies the load, and the surplus electricity is sent to the grid, if there is not enough renewable power, the energy to supply the demand is taken from the utility grid. This energy management is expressed in the Eq (22).

$$P_t^{Load} = \begin{cases} P_{ps,t}^{PV} + P_{ps,t}^{HKT} + P_{ps,t}^{g,s},\ P_{ps,t}^{PV} + P_{ps,t}^{HKT} \geq P_t^{Load} \\ P_{ps,t}^{PV} + P_{ps,t}^{HKT} + P_{ps,t}^{BSS-},\ P_{ps,t}^{PV} + P_{ps,t}^{HKT} < P_t^{Load} \text{ and } SOC_{ps,t}^{BSS} \geq \underline{SOC}_{ps,t}^{BSS} \\ P_{ps,t}^{PV} + P_{ps,t}^{HKT} + P_{ps,t}^{g,b},\ P_{ps,t}^{PV} + P_{ps,t}^{HKT} < P_t^{Load} \text{ and } SOC_{ps,t}^{BSS} < \underline{SOC}_{ps,t}^{BSS} \end{cases} \tag{22}$$

3. Results and discussions

The results of the simulations and laboratory test according to the proposed mathematical representation are discussed in this section. Fig. 7 shows the photographic representation of the laboratory equipment.

Fig. 7. Equipment used for power smoothing tests in the microgrid laboratory of the University of Cuenca.

3.1. Power smoothing results

The results of the power smoothing have been analyzed for different days of the year chosen randomly. Fig. 8 shows the comparison of each method for the chosen days. The power flow sent to the grid has rising and falling peaks which are corrected by the algorithms.

The power fluctuations also depend on the peaks of the electrical load, which can mean a high variation combined with the power output of the renewable sources. Fig. 9 shows the PV/HKT load and power profiles for three days.

3.2. Power smoothing comparison

The equipment shown in Table 1 belongs to the microgrid laboratory of the University of Cuenca. In this section, a comparison between the results of the laboratory and the simulations in Matlab - Simulink is presented. The objective of this analogy is to demonstrate the feasibility of working with simulated models, since it is more efficient and faster. Fig. 10 shows the results of the computational model with respect to the laboratory tests. It is logical that the results do not coincide perfectly, since the model does not consider aspects such as the dirtiness of the

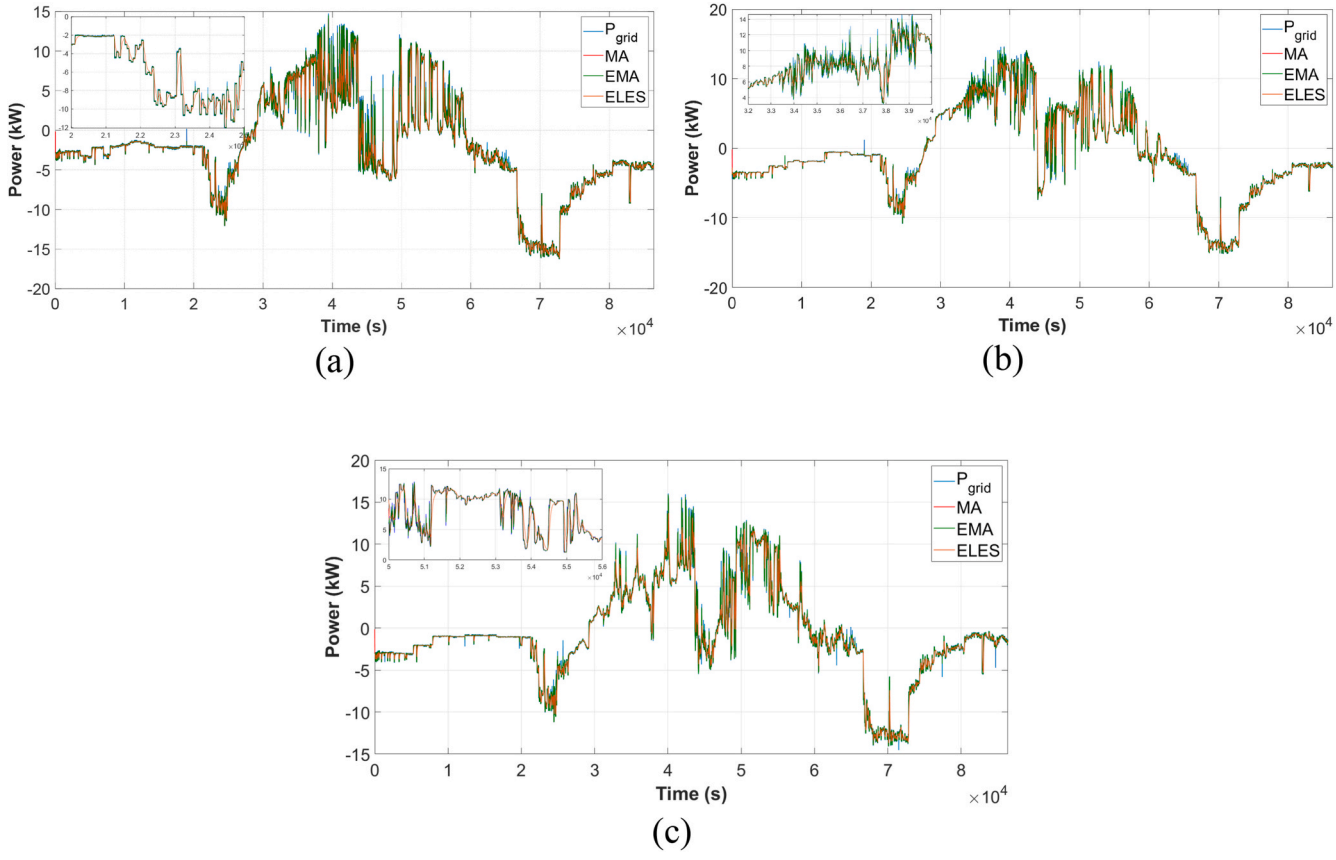

Fig. 8. Power smoothing results (a), (b) and (c) days 1, 2 and 3 respectively.

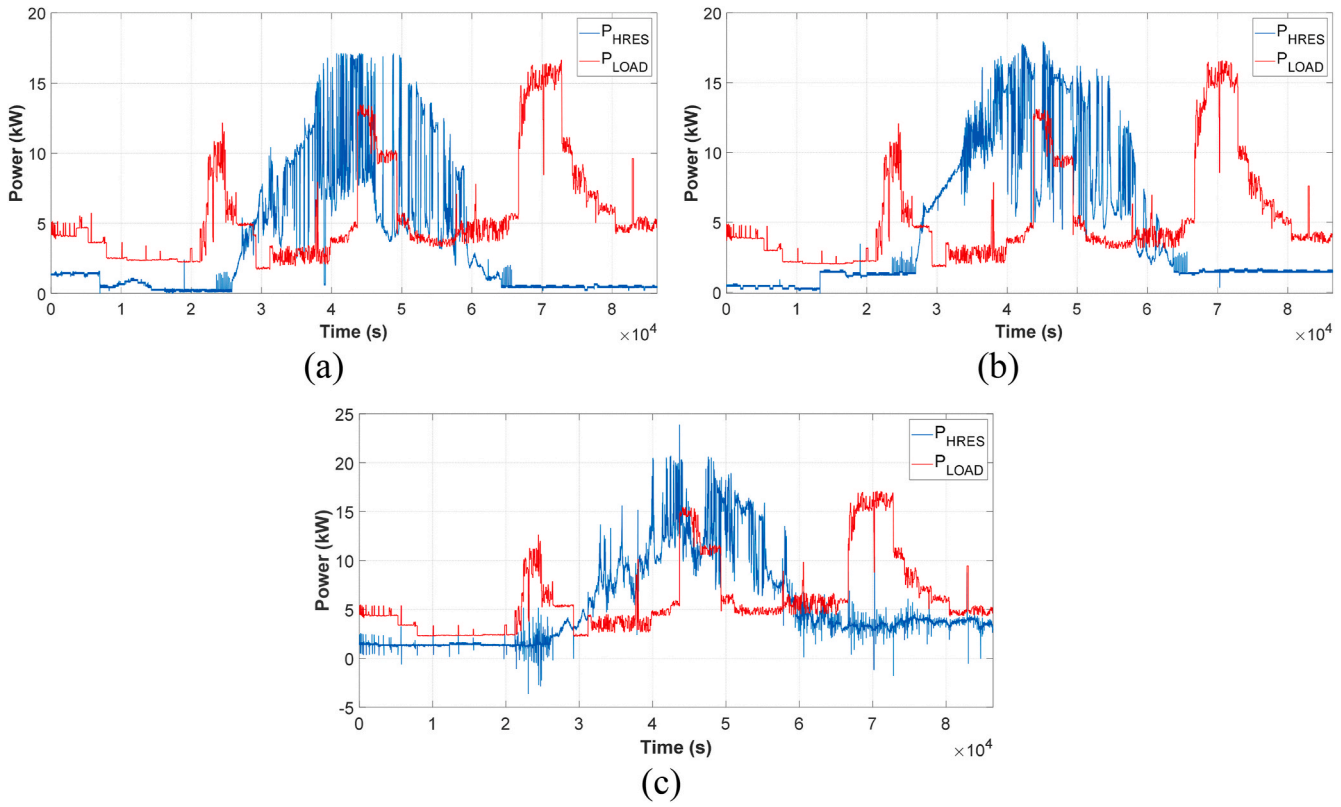

Fig. 9. Electric power flow for the HRES and load; (a), (b) and (c) for days 1, 2 and 3 respectively.

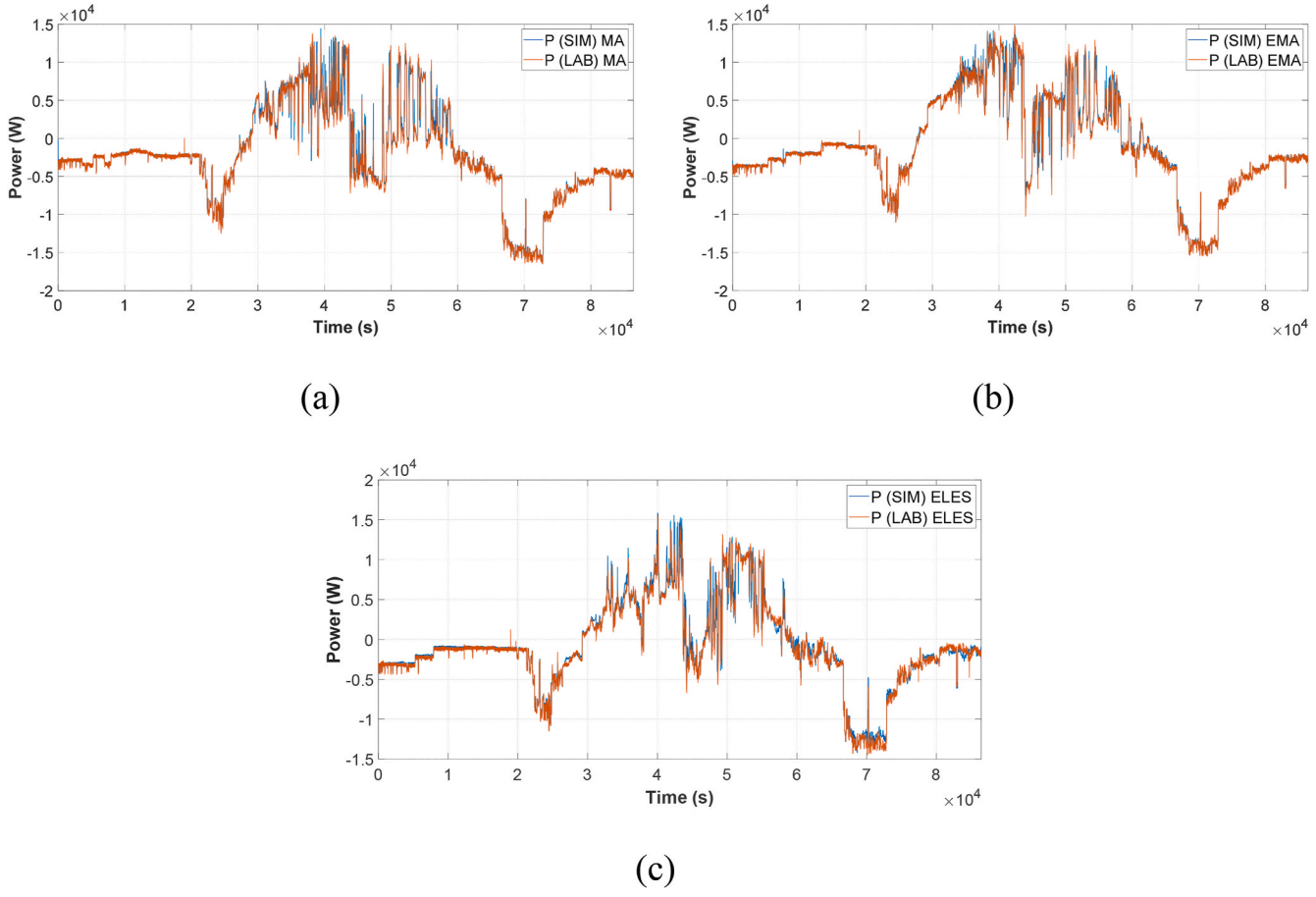

Fig. 10. Laboratory model accuracy relative to computer simulations; (a), (b), (c) day 1, 2 and 3 respectively.

Table 2
Determination of the accuracy of the computational model with laboratory tests.

Methods	MAE (W)	RMSE (W)	MAPE (%)
MA	443.57	918.08	3.15
EMA	402.69	831.24	2.82
ELES	487.94	830.47	2.40

Table 3
SC charge/discharge cycles under the proposed power smoothing methods, 24 h time window.

Day	Index	MA	EMA	ELES
Day #1	Charge	740	711	746
	Discharge	699	729	693
Day #2	Charge	714	718	732
	Discharge	720	715	707
Day #3	Charge	737	715	762
	Discharge	701	719	677

solar panels, the losses in the wires, the time constants and the efficiency of the equipment; the results approximate real conditions.

Based on the extensive literature reviewed, three ways of measuring the precision of the experiment and computer simulation have been chosen, the mean absolute error (MAE) [26], root mean square error (RMSE) [27] and mean absolute percentage error. (MAPE) [26], in this way it is possible to quantitatively calculate the precision of the model made in Matlab.

The errors of the prediction are determined by Eq. (23 – 25):

$$MAE = \frac{1}{n}\sum_{1}^{n}|X_s - X_l| \tag{23}$$

$$RMSE = \sqrt{\frac{1}{n}\sum_{1}^{n}(X_s - X_l)^2} \tag{24}$$

$$MAPE\ (\%) = \frac{1}{n}\sum_{1}^{n}\frac{|X_s - X_l|}{X_l} \times 100 \tag{25}$$

where: n is the time in seconds of testing, X_s and X_l are respectively the simulated (SIM) value and the laboratory (LAB) value. As expected, the absolute errors in terms of percentage are apparently high, when referring the errors to electrical power MAE (W), the values are of the order of 400 W referred to 25,000 W, in the case of EMA (W) the results are based on the square root of the square of the absolute errors, 850 W also referred to 25,000 W. The results are not high values. Finally, the relative MAPE error (W) is the smallest in the order of 3%. This result is shown in Table 2. It can be concluded that the laboratory tests fit the simulations in Matlab-Simulink.

3.3. Sensitivity análisis

3.3.1. SC charge/discharge cycles

The power smoothing methods proposed in this paper have been shown to reduce power oscillations successfully. However, the behavior of the SC under each of them has not yet been studied. In this section, a sensitivity analysis of the SC charge/discharge cycles under each proposed method is presented. Table 3 shows the results for the proposed days (see Fig. 4).

The useful life of an SC can be measured indirectly according to the number of charge/discharge cycles. In this sense, under the ELES method, the SC presents a greater number of charge/discharge cycles with respect to MA and EMA, respectively. Being the opposite behavior with respect to the number of discharge cycles, where under the EMA method the greatest number of events arise. To clarify this point, considering the number of charge/discharge cycles during the four days presented in Table 3, the highest number of cycles results from the ELES method with 5756 times, then under the MA method with 5748 times and finally the method that produces fewer charge/discharge cycles is EMA with 5740 times.

3.3.2. Battery and SC response to depth of discharge

The response of the SC to each power smoothing method is different, its SOC will vary depending on the algorithm, the measurement of the depth of discharge and the number of charges/discharges of the SC is useful if considering hybrid storage systems, since the response of BSS is usually slow, the graphical representation of the SOC for each proposed power smoothing method is shown in Fig. 11.

Despite the fact that the days of the experiment were consecutive and under the same conditions (completely clear sky). It is evident that the ELES method produces shallower charges/discharges, while the EMA method has a greater depth of discharge than the rest of the methods and the MA method has greater depths of charge. These results serve to determine the lifespan of the SC with respect to PV and HKT

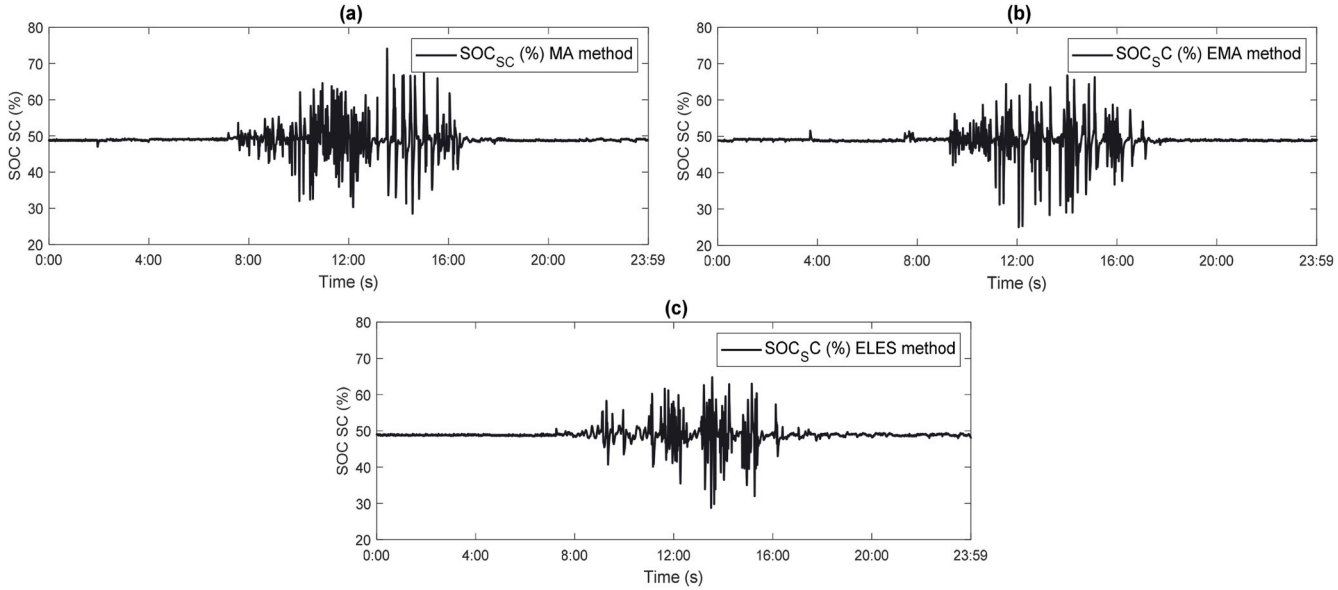

Fig. 11. State of charge (SOC) of supercapacitors: (a) Day 1, (b) Day 2 and (c) Day 3.

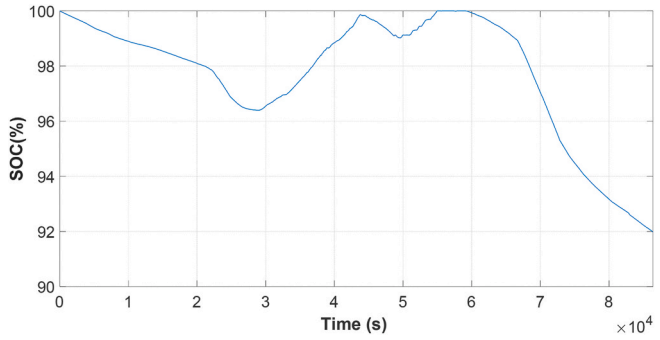

Fig. 12. SOC of BSS in day 1.

Table 4
Energy flow between customers load and the utility grid for one day, hourly average data.

Time (h)	To Grid HKT/SC/BAT/Grid (Wh)	From Grid HKT/SC/BAT/Grid (Wh)	To Grid HKT/SC/Grid (Wh)	From Grid HKT/SC/Grid (Wh)
0–1	0.00	0.00	0.00	2859.0
1–2	0.00	0.00	0.00	2848.0
2–3	0.00	0.00	0.00	2221.0
3–4	0.00	0.00	0.00	1632.0
4–5	0.00	0.00	0.00	2196.0
5–6	0.00	0.00	2.812 e^{-3}	2267.0
6–7	0.00	0.00	0.00	7746.0
7–8	0.00	0.00	5.30	2724.0
8–9	0.00	0.00	3673.0	2.17
9–10	0.00	0.00	5622.0	0.895
10–11	0.00	0.00	6988.0	135
11–12	0.00	0.00	5990.0	0,00
12–13	0.00	0.00	1747.0	2856.0
13–14	0.00	0.00	1001.0	3487.0
14–15	1376.0	0.00	3922.0	54.2
15–16	1015.2	0.00	3498.0	73.2
16–17	0.00	0.00	1120.0	1377.00
17–18	0.00	0.00	0.00	3468.00
18–19	0.00	0.00	0.00	8827.00
19–20	0.00	0.00	0.00	14,720.0
20–21	0.00	0.00	0.00	10,450.0
21–22	0.00	0.00	0.00	6438.00
22–23	0.00	0.00	0.00	4587.00
23–24	0.00	0.00	0.00	4712.00
Total	2391.20	0.00	33,566.30	85,680.46

fluctuations. Therefore, the SC helps to reduce the charge/discharge oscillations in the BSS. Fig. 12 shows the SOC (%) of BSS for day 1 as an example.

3.3.3. Cost of energy

In this section, daily economic analysis to study the impact of BSS in residential system is performed. Day 1 is taken as an example, where through Eq. (22) the energy flow between the customers load (electricity demand) and the utility grid has been calculated, these results are shown in Table 4.

To calculate the energy cost, it is necessary to know the price of electricity (kWh) for sale and purchase with the utility grid. In Ecuador, there is currently no well-defined regulation for the price of renewable energies. Therefore, the price of mini-hydroelectric plants (less than 5 MW) is considered as a reference to HKT 0.0658 USD/kWh, for solar

Table 5
Daily energy cost for systems with and without BSS respectively.

Flow	HKT/SC/BAT/Grid	HKT/SC/Grid
To grid	15.73 cUSD/kWh	2.20 USD/kWh
Fom grid	–	8.14 USD/kWh

Table 6
Energy balance of the utility grid with respect to the variation of BSS capacity.

BSS Capacity (kWh)	To Grid HKT/SC/BSS/Grid (Wh-day)
30	2145.56
50	2210.03
100	2380.89
200	2382.54
300	2385.23
400	2387.50
436.56	2389.20
500	2392.35

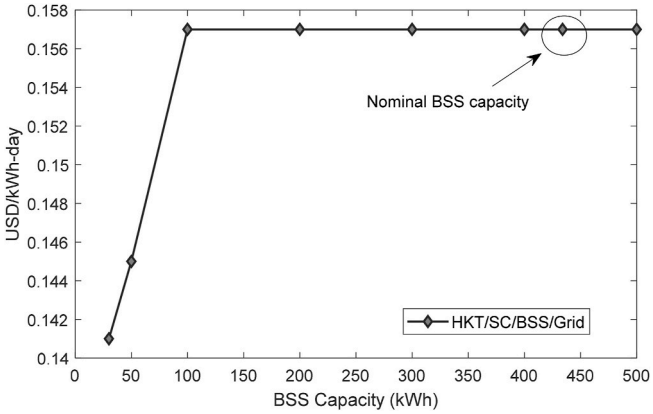

Fig. 13. Cost of energy sent to the grid for day 1. Values for different BSS capacities.

energy a rate has not been considered since it does not exist in Ecuador [28]. The Feed in Tariff (FIT) (Regulation No. CONELEC 001/13) did not contemplate any price for PV/HKT. Besides, according to Ref. [29], the cost of energy for the residential sector in Ecuador is considered 0.095 USD/kWh. Therefore, the results of cost of energy (USD/kWh-day) are shown in Table 5.

It is evident that the BSS avoids buying energy from the utility grid for this day under study, the surplus electricity represents a net profit for the consumer. If BSS is not considered, high energy is sold to the grid, however the energy purchased is greater and more expensive. Therefore, this system is economically less feasible.

3.3.4. Effect of the size of BSS and SC

Sizing variations of the HESS would affect the amount of energy to/from the utility grid and the SOC of BSS. Due to the configuration and energy control of the HRES, the size of the SC should not affect the energy and economic results (only the capital cost), since the primary objective of the SC is to reduce energy fluctuations and not to store energy in the long term as BSS. To determine this premise, this section presents a sensitivity analysis of HESS capacity with respect to SOC and associated energy costs. Considering the nominal capacity of BSS is 436.56 kWh. Table 6 shows the energy result of different BSS capacities. For this analysis, day 1 and the ELES power smoothing method have been used.

It is evident that the BSS prevents energy from being purchased from the utility grid for day 1, which is analyzed in this case. It is apparent that by increasing the BSS capacity, the energy sent to the grid is greater. When calculating the energy cost of the energy sent to the grid, the curve shown in Fig. 13 is obtained.

Fig. 13 shows that the increase in net profit to consumers is greater for the first two steps (30 kWh and 50 kWh) since the capacity of BSS with respect to renewable production is considerable. However, for subsequent increases in BSS capacity, the cost does not vary significantly because renewable production is constant PV/HKT. This reflects that if

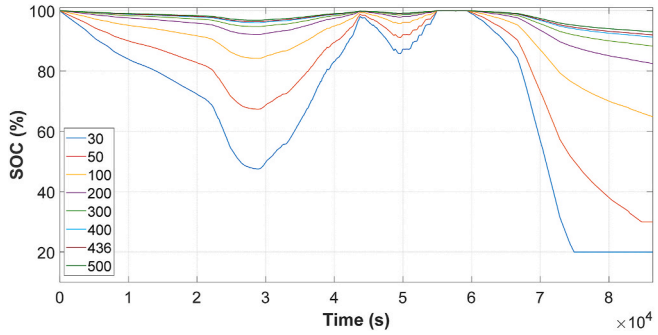

Fig. 14. State of load (SOC) for different BSS capacities during day 1.

the BSS is oversized, the energy cost is not exactly higher. Therefore, it would not represent significant profits for consumers. On the other hand, if the BSS is undersized, the depth of discharge (DOD) could be very low and shorten the lifespan of the batteries. Fig. 14 shows the SOC for different BSS capacities during day 1.

The BSS response for relatively low capacities (30 kWh and 50 kWh) is a deep DOD, less than 20% of the SOC for the first case. As the BSS capacity increases, the SOC is flatter. It is important to mention that if the BSS work in a higher SOC band, their lifespan increases and it is not recommended to operate with SOC less than 20% for lithium ion batteries [30–33]. To avoid the oversizing of the BSS, in this paper the lowest capacity of the BSS has been chosen for a minimum SOC of 20% for a whole year, this capacity is 436.56 kWh. The annual SOC in BSS

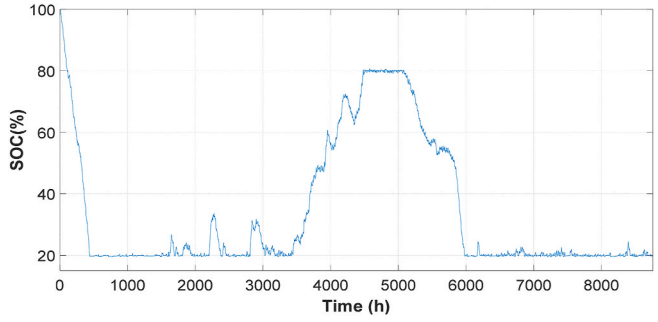

Fig. 15. Annual State of Charge of BSS with a capacity of 436.56 kWh

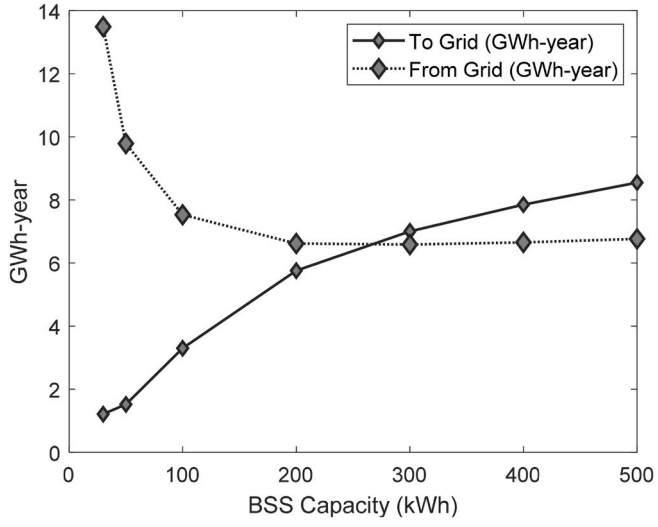

Fig. 16. Rate of change of the annual energy exchange with respect to the increase in the capacity of BSS.

with this capacity is shown in Fig. 15. The annual SOC in BSS with this capacity is shown in Fig. 15. It is evident that when analyzing the annual SOC, the behavior is different with respect to daily SOC, this result is analyzed in an hourly time interval, where the power smoothing is not evident since there are power fluctuations that last seconds.

When analyzing the annual energy exchange with the utility grid, the results show the response of the system with respect to variations in BSS capacities. The result clearly shows a reduction in power from the grid if the BSS capacity is increased. Likewise, at higher energy storage capacities, the energy sent to the grid increases. It is important to mention that the rate of change in both cases is different, as shown in Fig. 16.

The annual net profit for different BSS capacities is shown in Fig. 17 it is evident that while the storage capacity is greater, the cost tends to remain constant.

On the other hand, in this paper the optimal capacity of SC has been calculated using Eq. (3) (130 F) considering the duration and maximum value of the largest power fluctuation according to the annual data in Fig. 2. If the SC capacity increases, the stored energy will be the same due to the energy management presented in Eq. (22). The objective of SC is to flatten the rise and fall peaks and not increase self-consumption. But

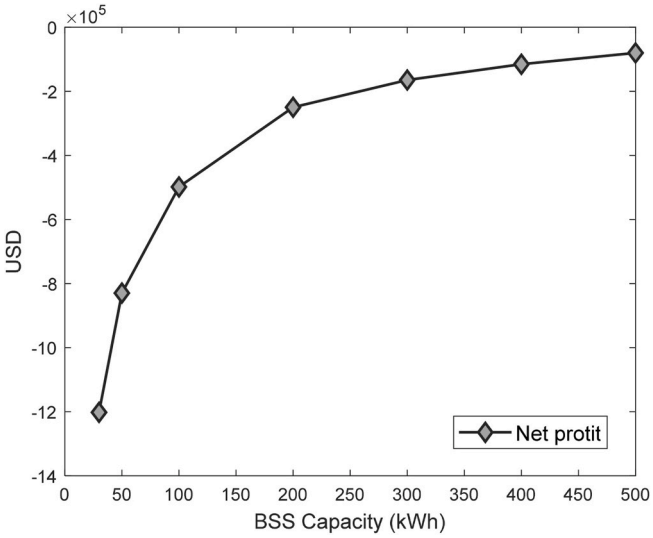

Fig. 17. Annual net profit of consumers with respect to the increase in BSS capacity.

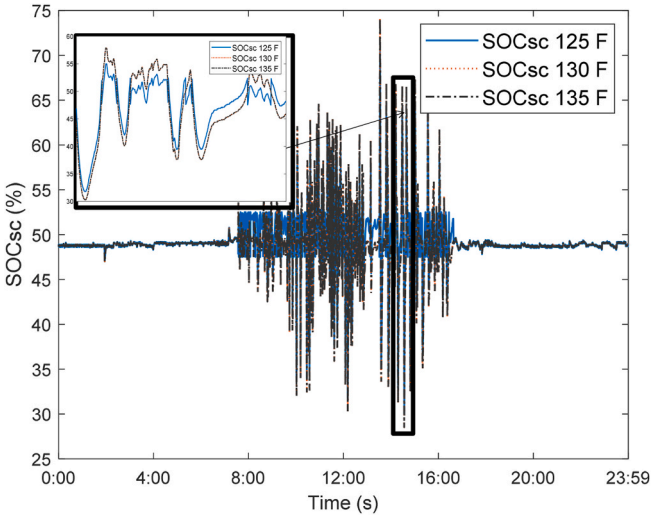

Fig. 18. Variation of SC capacity with respect to SOC. Power smoothing method used (ELES) values for day 1.

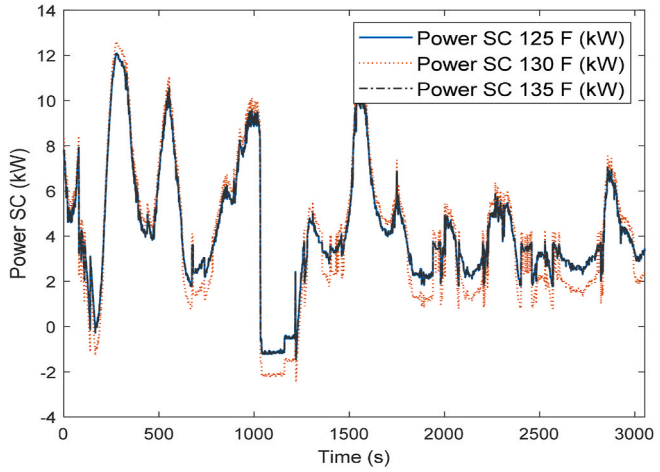

Fig. 19. SC output power smoothing for different energy storage capacities.

if the SC capacity is reduced, the response of the power smoothing system could show different patterns. In this context, simulations have been performed varying the SC capacity as shown in Fig. 18. For this section, data from day 1 with the ELES power smoothing method have been used. Therefore, the SOC for a 125 F rated SC has a lower power smoothing band. On the contrary, by increasing the capacity to 135 F, the power smoothing band remains constant. In summary, increasing SC capacity does not produce greater energy exchanges with the grid.

The reduction of the power smoothing band by decreasing the SC capacity causes a lower response to power fluctuations. Fig. 19 demonstrates this hypothesis, the SC of 125 F has less capacity to reduce power peaks than SC of 130 F, while the supercapacitor of 135 F has the same power smoothing capacity with respect to SC 130 F. The results of day 1 (12:00–12:40 p.m.) using the ELES power smoothing algorithm have been using.

3.3.5. *Voltage profiles at PCC*

The stability of the voltage in the electrical grid is considered a key parameter for renewable systems, since it has high PV/HKT fluctuations, it is necessary to reduce the voltage profile avoiding compromising the utility grid in the event of possible tension fall. In this case, the power smoothing algorithms regulate the voltage at the PCC point as shown in Fig. 20.

In order to measure the efficiency of voltage regulation, it has been proposed to analyze the flicker index. The flicker (P_{st}) is analyzed according to the IEC 61000-4-15 standard [26] and is calculated with Eq. (26) and must be less than unity [34].

$$P_{st} = \sqrt{0.0314P_{0.1} + 0.0525P_1 + 0.0657P_3 + 0.028P_{10} + 0.08P_{50}} \tag{26}$$

where:

P_{st}, short duration flicker severity index.

$P_{0.1}$, P_1, P_3, P_{10}, P_{50} are the index levels greater than 0.1%, 1%, 3%, 10%, 50% of the total time of the measurement time window. Thus, when considering a HESS system formed by batteries and supercapacitors, the value of the flicker index is below unity, this complies with the values according to the IEC standard IEC 61000-4-15.

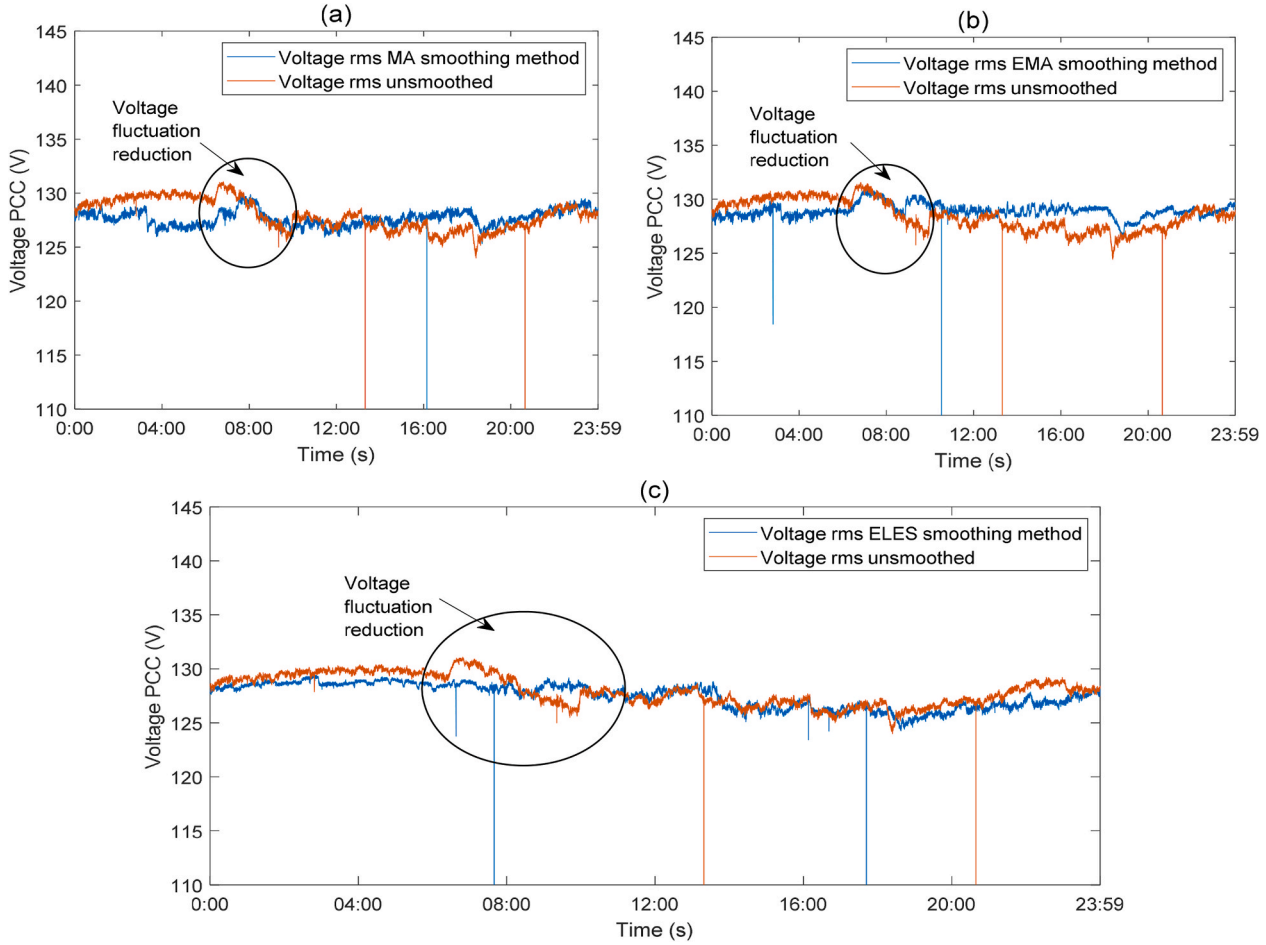

Fig. 20. Voltage in PCC, values taken in phase A in alternating current.

4. Conclusion

A feasibility analysis of three power smoothing methods for a renewable PV/HKT system has been done through laboratory tests. The algorithms are based on a hybrid energy storage system (SC/BSS), for which various studies have been carried out based on technical and economic indices, the time interval studied is 1 s and three days have been chosen randomly.

The ELES method shows a better behavior against PV/HKT power fluctuations, reducing the rising and falling peaks, the EMA method effectively reduces the falling peaks. However, the rising peaks are higher than the ELES method. On the other hand, the MA method shows an inverse behavior to the EMA, since it is effective in reducing the rising peaks, nevertheless, in the falling peaks it shows lower performance with respect to ELES.

If the simulation models are compared with the laboratory tests, the lowest relative error is shown by the ELES method and the highest error is presented by the MA method with 3.15%. These results show the importance of working with computational models based on laboratory parameters, since the results are numerically similar.

When analyzing the number of charge/discharge cycles in the SCs for the three proposed days, the highest number of cycles results from the ELES method with 5756 times, then under the MA method with 5748 times and finally the method that produces fewer charge/discharge cycles is EMA with 5740 times. Additionally, when analyzing the SOC of the SC under the proposed power smoothing methods, the ELES method presents shallower charges/discharges. These results serve to determine the lifespan of the SCs in the face of photovoltaic and hydrokinetic fluctuations.

From the economic point of view, it is feasible to use BSS/SC rather than just SC, since the net profit for the consumer is 15.73 cUSD/kWh-day and without BSS it has a consumption of 5.21 USD/kWh-day, these analyzes do not consider capital cost.

The sensitivity study with respect to BSS capacity showed that the minimum state of charge is an important factor in determining the optimal size of the batteries. If the capacity of BSS is increased, the net profits from the energy exchange with the grid are not feasible. Likewise, the optimal capacity of the SC is determined with respect to the maximum power peaks throughout the year and their time interval. By reducing the SC capacity, the response to power fluctuations is affected, on the other hand, by increasing the SC capacity, the energy exchange with the grid and the response to power smoothing is the same.

Finally, the voltage response in PCC has been studied, when using the power smoothing algorithms with SC, the flicker is under the unit according to IEC standard IEC 61000-4-15.

Declaration of competing interest

The authors declare that they have no known competing financial interests or personal relationships that could have appeared to influence the work reported in this paper.

Data availability

Data will be made available on request.

Acknowledgment

The author (Paul Arévalo) thanks the Call for Grants for the Requalification of the Spanish University System for 2021–2023, Margarita Salas Grants for the training of young doctors awarded by the Ministry of Universities and financed by the European Union –NextGenerationEU.

The authors thank Universidad de Cuenca for easing access to the facilities of the Microgrid Laboratory of the Centro Científico Tecnológico y de Investigación Balzay (CCTI-B), for allowing the use of its equipment, and for authorizing its staff the provision of technical support necessary to carry out the experiments described in this article.

The icons used in this document were developed by Freepik, monkik, Smashicons and Pixel perfect, from www.flaticon.com.

References

[1] L.H. Vera, M. Cáceres, A. Busso, Grid connected photovoltaic systems to the urban environment of argentinian northeast, Energy Proc. 57 (2014) 3171–3180, https://doi.org/10.1016/J.EGYPRO.2015.06.066.

[2] Y. Chang, X. Mao, Y. Zhao, S. Feng, H. Chen, D. Finlow, Lead-acid battery use in the development of renewable energy systems in China, J. Power Sources 191 (1) (2009) 176–183, https://doi.org/10.1016/J.JPOWSOUR.2009.02.030.

[3] P. Saini, L. Gidwani, An investigation for battery energy storage system installation with renewable energy resources in distribution system by considering residential, commercial and industrial load models, J. Energy Storage 45 (2022), 103493, https://doi.org/10.1016/J.EST.2021.103493.

[4] D. Lamsal, V. Sreeram, Y. Mishra, D. Kumar, Output power smoothing control approaches for wind and photovoltaic generation systems: a review, Renew. Sustain. Energy Rev. 113 (2019), 109245, https://doi.org/10.1016/J.RSER.2019.109245.

[5] R.A. Thokar, N. Gupta, K.R. Niazi, A. Swarnkar, N.K. Meena, Multiobjective nested optimization framework for simultaneous integration of multiple photovoltaic and battery energy storage systems in distribution networks, J. Energy Storage 35 (2021), 102263, https://doi.org/10.1016/J.EST.2021.102263.

[6] M.A. Syed, M. Khalid, Neural network predictive control for smoothing of solar power fluctuations with battery energy storage, J. Energy Storage 42 (2021), 103014, https://doi.org/10.1016/J.EST.2021.103014.

[7] W. Ma, W. Wang, X. Wu, R. Hu, F. Tang, W. Zhang, Control strategy of a hybrid energy storage system to smooth photovoltaic power fluctuations considering photovoltaic output power curtailment, Sustain. Times 11 (5) (2019) 1324, https://doi.org/10.3390/SU11051324, 2019.

[8] W. Ma, W. Wang, X. Wu, R. Hu, F. Tang, W. Zhang, X. Han, L. Ding, Optimal allocation of hybrid energy storage systems for smoothing photovoltaic power fluctuations considering the active power curtailment of photovoltaic, IEEE Access 7 (2019) 74787–74799, https://doi.org/10.1109/ACCESS.2019.2921316.

[9] M.S. Masaki, L. Zhang, X. Xia, A hierarchical predictive control for supercapacitor-retrofitted grid-connected hybrid renewable systems, Appl. Energy 242 (2019) 393–402, https://doi.org/10.1016/J.APENERGY.2019.03.049.

[10] G. Wang, M. Ciobotaru, V.G. Agelidis, Power smoothing of large solar PV plant using hybrid energy storage, IEEE Trans. Sustain. Energy 5 (3) (2014) 834–842, https://doi.org/10.1109/TSTE.2014.2305433.

[11] S. Ali, G. Khalil, A.A. Bidram, C. Seyyed, A. Ghorashi, K. Abadi, A distributed rule-based power management strategy in a photovoltaic/hybrid energy storage based on an active compensation filtering technique, IET Renew. Power Gener. 15 (15) (2021) 3688–3703, https://doi.org/10.1049/RPG2.12263.

[12] Y. Jiang, J. Fletcher, P. Burr, C. Hall, B. Zheng, D.W. Wang, Z. Ouyang, A. Lennon, Suitability of representative electrochemical energy storage technologies for ramp-rate control of photovoltaic power, J. Power Sources 384 (2018) 396–407, https://doi.org/10.1016/J.JPOWSOUR.2018.03.013.

[13] S. Sukumar, M. Marsadek, K.R. Agileswari, H. Mokhlis, Ramp-rate control smoothing methods to control output power fluctuations from solar photovoltaic (PV) sources—a review, J. Energy Storage 20 (2018) 218–229, https://doi.org/10.1016/J.EST.2018.09.013.

[14] V. Tzelepis, J.H. Van Zwieten, N.I. Xiros, C. Sultan, System modeling and simulation of in-stream hydrokinetic turbines for power management and control, J. Dyn. Syst. Meas. Control. Trans. ASME. 139 (5) (2017), 051005, https://doi.org/10.1115/1.4035235/384636.

[15] A.H. Birjandi, E.L. Bibeau, Frequency analysis of the power output for a vertical axis marine turbine operating in the wake, Ocean Eng. 127 (15) (2016) 325–334, https://doi.org/10.1016/J.OCEANENG.2016.09.045.

[16] J.L. Espinoza, L.G. Gonzalez, R. Sempertegui, Micro grid laboratory as a tool for research on non-conventional energy sources in Ecuador, 2017 IEEE Int. Autumn Meet. Power, Electron. Comput. ROPEC 2018 (2018-January) (2017) 1–7, https://doi.org/10.1109/ROPEC.2017.8261615.

[17] Network of meteorological and hydrological stations. National Institute of Meteorology and Hydrology (INAMHI). https://inamhi.wixsite.com/inamhi/novedades (accessed May 26, 2022).

[18] M. Tostado-Véliz, P. Arévalo, F. Jurado, An optimization framework for planning wayside and on-board hybrid storage systems for tramway applications, J. Energy Storage 43 (2021), 103207, https://doi.org/10.1016/J.EST.2021.103207.

[19] P. Arévalo, A. Cano, J. Benavides, F. Jurado, Feasibility study of a renewable system (PV/HKT/GB) for hybrid tramway based on fuel cell and super capacitor, IET Renew. Power Gener. 15 (3) (2021) 491–503, https://doi.org/10.1049/RPG2.12056.

[20] A. Cano, P. Arévalo, D. Benavides, F. Jurado, Sustainable tramway, techno-economic analysis and environmental effects in an urban public transport. A comparative study, Sustain. Energy, Grids Networks. 26 (2021), 100462, https://doi.org/10.1016/J.SEGAN.2021.100462.

[21] D. Lin, X. Li, S. Ding, Y. Du, Strategy comparison of power ramp rate control for photovoltaic systems, CPSS Transactionson Power Electronics and Applications 5 (4) (2020) 329–341, https://doi.org/10.24295/CPSSTPEA.2020.00027.

[22] J.F. Patarroyo-Montenegro, J.D. Vasquez-Plaza, O.F. Rodriguez-Martinez, Y.V. García F. Andrade, Comparative and cost analysis of a novel predictive power ramp

rate control method: a case study in a PV power plant in Puerto Rico, Appl. Sci. 11 (13) (2021) 5756, https://doi.org/10.3390/app11135766.
[23] R. Kini, D. Raker, T. Stuart, R. Ellingson, M. Heben, R. Khanna, Mitigation of PV variability using adaptive moving average control, IEEE Trans. Sustain. Energy 11 (4) (2019) 2252–2262, https://doi.org/10.1109/TSTE.2019.2953643.
[24] J.G. Silva, J.O.L. Filho, E.L.F. Fortaleza, Adaptive extended kalman filter using exponencial moving average, IFAC-Papers On Line 51 (25) (2018) 208–211, https://doi.org/10.1016/j.ifacol.2018.11.106.
[25] U. Ekasit, S. Siriroj, H. Natchpong, H. Makoto, A case study in micro grid using adaptive enhanced linear exponential smoothing technique, in: 8th International Conference on Information and Communication Technology for Embedded Systems, IC-ICTES 2017 – Proceedings, 2017, https://doi.org/10.1109/ICTEMSYS.2017.7958776.
[26] M. Arnaud, G. Boris, L.G. Bénédicte, R. Fabrice, Mean absolute percentage error for regression models, Neurocomputing 192 (2016) 38–48, https://doi.org/10.1016/J.NEUCOM.2015.12.114.
[27] C. Martin, Shady.H.E.A. Aleem, Z. Ahmed F, On the root mean square error (RMSE) calculation for parameter estimation of photovoltaic models: a novel exact analytical solution based on Lambert W function, Energy Convers. Manag. 210 (2020), 112716, https://doi.org/10.1016/J.ENCONMAN.2020.112716.
[28] N.G. Jara Cobos, F.Z. Reinoso Avecillas, C.A. Isaza Roldan, J.L. Espinoza Abad, Impacts on the consumption of electric power by the use of efficient refrigerators - Ecuador case, Ingenius (2017) 53–63, https://doi.org/10.17163/INGS.N18.2017.07.
[29] J.P. Muñoz-Vizhñay, M.V. Rojas-Moncayo, C.R. Barreto-Calle, Incentive pertaining to energy the generation distributed in Ecuador, Ingenius 19 (2018) 60–68, https://doi.org/10.17163/INGS.N19.2018.06.
[30] J. Su, M. Lin, S. Wang, J. Li, J. Coffie-Ken, F. Xie, An equivalent circuit model analysis for the lithium-ion battery pack in pure electric vehicles, Meas. Control 52 (2019) 193–201, https://doi.org/10.1177/0020294019827338.
[31] C. Brivio, V. Musolino, M. Merlo, C. Ballif, A physically-based electrical model for lithium-ion cells, IEEE Trans. Energy Convers. 34 (2019) 594–603, https://doi.org/10.1109/TEC.2018.2869272.
[32] W. Li, Y. Fan, F. Ringbeck, D. Jöst, X. Han, M. Ouyang, D.U. Sauer, Electrochemical model-based state estimation for lithium-ion batteries with adaptive unscented Kalman filter, J. Power Sources 476 (2020), https://doi.org/10.1016/J.JPOWSOUR.2020.228534.
[33] S.G. Tesfahunegn, Ulleberg, P.J.S. Vie, T.M. Undeland, Optimal shifting of Photovoltaic and load fluctuations from fuel cell and electrolyzer to lead acid battery in a Photovoltaic/hydrogen standalone power system for improved performance and life time, J. Power Sources 196 (2011) 10401–10414, https://doi.org/10.1016/J.JPOWSOUR.2011.06.037.
[34] A. Cano, P. Arévalo, F. Jurado, Evaluation of temporal resolution impact on power fluctuations and self-consumption for a hydrokinetic on grid system using supercapacitors, Renew. Energy 193 (2022) 846–856, https://doi.org/10.1016/j.renene.2022.05.070.